Pramana – J. Phys. (2019) 93:11
https://doi.org/10.1007/s12043-019-1769-4

Quantum coupling and electrothermal effects on electron transport in high-electron mobility transistors

LING-FENG MAO

School of Computer and Communication Engineering, University of Science and Technology Beijing, 30 Xueyuan Road, Haidian District, Beijing 100083, People's Republic of China
E-mail: mail_lingfeng@aliyun.com, lingfengmao@ustb.edu.cn

MS received 23 March 2018; revised 17 December 2018; accepted 20 December 2018; published online 8 May 2019

Abstract. Based on the energy and momentum balance equations and three-dimensional Schrödinger equations, a physical model of the quantum coupling and electrothermal effects on the electron transport in GaN transistors is proposed. Quantum coupling and electrothermal effects in GaN transistors cause a reduction in the barrier height, changes in the quantised energy levels of the two-dimensional electron gas, and a decrease in the electron density and source–drain current. This model predicts that the current collapse in GaN transistors can occur under channel electrons with large transverse energy and it can be alleviated by optimising the physical device parameters. The gate length-dependent resistance predicted by the proposed model agrees well with the experimental data reported in the literature. Not only the physical mechanism but also the possibility to improve the reliability of high-electron mobility (HEMT) GaN transistors by optimising its physical parameters has been given in this model due to its analytic nature.

Keywords. Quantum coupling; electrothermal effects; quantisation; electron transport; GaN transistor.

PACS Nos 73.23.–b; 73.40.Qv; 73.50. –b

1. Introduction

The GaN high-electron mobility transistor (HEMT) has recently emerged in the application of switch and radiofrequency electronics [1–13]. The reliability of GaN HEMTs is a major concern for its application. Current collapse, a temporary reduction of source–drain current when high power or/and high voltage is applied, is often observed in the fabricated GaN HEMTs, which ultimately limits their output power density. In order to explain the current collapse in GaN HEMTs, the concept of 'virtual gate' was introduced. This is a phenomenon in which electrons are captured by the traps at the corner of the gate [2], and the two-dimensional electron gas depletion caused by the capture behaviour of the surface (donor) states decreases the source–drain current [6]. For suppressing the current collapse in GaN HEMTs, bilayer gate dielectric [7], multifield plate structures [8], passivation treatment [9] and surface treatment [10] have been introduced during the fabrication of GaN HEMTs. Classical examples of hot-electron effects and the current collapse in GaN HMETs can be found in [14–16]. For suppressing the current collapse phenomenon in the GaN HMETs, it is better to understand its physical mechanism. Developing a physical picture to explain the current collapse in GaN HEMTs is helpful to understand how it limits the reliability of GaN HEMTs. Thus, any effort made to understand the current collapse in GaN HEMTs deserves further study.

Hot-electron phenomena, determined by the momentum and energy relaxation, are very important for physically understanding all modern semiconductor devices. The momentum relaxation in modern semiconductor devices is dominated by elastic collisions in hot-electron transport, whereas the energy relaxation is determined by inelastic interactions with phonons. As gate lengths in transistors shrink, the non-equilibrium nature of electrons has more pronounced effects on the performance of transistors [17]. The electron temperature is found to be much higher than the lattice temperature in GaN HEMTs [18]. A very large electron temperature can result in a decrease in the channel electron density of GaN HEMTs [19], make an important contribution to the gate leakage current in graphene transistors [20], have a large effect on the effective activation energy in organic transistors [21], have a large effect on the short channel effects

in nanoscale silicon transistors [22] and also shift the spectra of Raman photo- and electro-luminescence of graphene-related electronic devices [23]. At the same time, the fact that hot electrons can cause a significant current collapse has been observed in the experiments in GaN HEMTs [24].

The two-dimensional electron gas is confined to the AlGaN–GaN interface in a conventional GaN HEMT, which can lead to the energy quantisation of the electron motion along the direction perpendicular to the AlGaN–GaN interface. Such an energy quantisation will redistribute the channel electrons, and thus has a significant influence on the performance of the GaN-based HEMTs. With the help of the solution to the coupled Poisson and Schrödinger equations, the quantum feature of the channel electrons in the GaN HEMTs could physically be understood. One can note that the one-dimensional parabolic band effective-mass theory is often used to study the quantum feature of the device performance. The one-dimensional parabolic band effective-mass theory implies the approximation that there is no quantum coupling among the components of electron motions in three directions. Additionally, one can note that the quantum coupling due to the effective electron mass mismatch at the heterojunction interface in a transistor can lead to an overestimation of effective barrier height [25–31]. The tunnelling current in the experiments is much higher than the theoretical prediction which is based on quantum coupling, neglecting the hot-electron effect [32]. This implies that the impacts of the reduction in the barrier height caused by the hot-electron effects of channel electrons on the energy quantisation cannot be neglected when the electron energy is large enough. All these imply that both the quantum coupling and hot-electron effects should be consolidated and taken into consideration in the modelling of modern semiconductor devices. Electronic traps and electron–phonon interaction were considered as major reasons for current collapse [33,34]. Successful suppression of current collapse by injecting holes was reported in [35]. Note that both electronic traps and electron–phonon interaction can affect the momentum and energy relaxation process which determine the hot-electron effect implying that hot-electron effects include both effects.

The purpose of this paper is to shed some light on how to physically understand the current collapse mechanism in GaN HEMTs with the help of the combination of quantum coupling and electrothermal effects (the energy relaxation of the channel electrons). The proposed model can clearly demonstrate the possible physical origin of the current collapse in GaN HEMTs through its simplicity and analytic nature.

2. Theory

The motion of the electrons in the channel of a transistor is determined by [36]

$$\frac{\mathrm{d}E}{\mathrm{d}t} = q\vec{v}\cdot\vec{F} - \frac{E-(3/2)k_{\mathrm{B}}T_{\mathrm{L}}}{\tau_{\mathrm{e}}}, \tag{1}$$

$$\frac{\mathrm{d}\vec{p}}{\mathrm{d}t} = q\vec{F} - \frac{\vec{p}}{\tau_{\mathrm{m}}}, \tag{2}$$

where T_{L} is the lattice temperature, q is the electron charge, $\vec{F}$ is the applied electric field along the channel, k_{B} is the Boltzmann constant, τ_{e} is the energy relaxation time, τ_{m} is the momentum relaxation time, E is the carrier energy, $\vec{p}$ is the carrier momentum and $\vec{v}$ is the carrier velocity along the channel. Under the steady-state conditions, eqs (1) and (2) can be rewritten as

$$E = q\vec{v}\cdot\vec{F}\tau_{\mathrm{e}} + \frac{3}{2}k_{\mathrm{B}}T_{\mathrm{L}} = \frac{3}{2}k_{\mathrm{B}}T_{\mathrm{e}}, \tag{3}$$

$$\vec{v} = \frac{q\vec{F}\tau_{\mathrm{m}}}{m^*} = \mu_{\mathrm{e}}\vec{F}, \tag{4}$$

where T_{e} is the carrier temperature, m^* is the effective mass of the carrier and μ_{e} is the carrier mobility. When a channel electric field (F_{ch}) is applied, the transversal kinetic energy (E_{tr}) of the channel electrons in the plane parallel to AlGaN–GaN interface is

$$\begin{aligned} E_{\mathrm{tr}} &= qvF_{\mathrm{ch}}\tau_{\mathrm{e}} + k_{\mathrm{B}}T_{\mathrm{L}} = \frac{q^2\tau_{\mathrm{m}}\tau_{\mathrm{e}}(F_{\mathrm{ch}})^2}{m^*} + k_{\mathrm{B}}T_{\mathrm{L}} \\ &= q\mu_{\mathrm{e}}\tau_{\mathrm{e}}(F_{\mathrm{ch}})^2 + k_{\mathrm{B}}T_{\mathrm{L}} = \frac{1}{2}m^*v^2 + k_{\mathrm{B}}T_{\mathrm{L}}. \end{aligned} \tag{5}$$

The Schrödinger equation of a GaN HEMT whose schematic cross-section and band diagram are shown in figure 1 under the circular cylindrical coordinates similar to those in silicon transistors [26–31] is

$$\begin{aligned} \Bigg[\frac{-\hbar^2}{2m_{\perp}(z)}\left(\frac{1}{r}\frac{\partial}{\partial r}\left(r\frac{\partial}{\partial r}\right) - \frac{\hbar^2}{r^2}\frac{\partial^2}{\partial\theta^2}\right) \\ -\frac{\hbar^2}{2m_z(z)}\frac{\partial^2}{\partial z^2} + \varphi(z)\Bigg]\xi(z) = E\xi(z), \end{aligned} \tag{6}$$

where E is the total electron energy, $\hbar$ is the reduced Planck's constant, z direction is the direction perpendicular to the AlGaN–GaN interface, $U(z)$ is the potential barrier along the z direction, $\xi(z)$ is the wave function along the z direction, r is the transverse coordinate in the plane parallel to the GaN–AlGaN interface, θ is the azimuth and $m_{\perp}$ and m_z denote the effective electron mass parallel and perpendicular to the GaN–AlGaN interface at the position of z, respectively. Note that $\left[\widehat{p}_{\perp}, \widehat{H}\right] = 0$ according to eq. (6) ($\widehat{p}_{\perp}$ is the electron momentum operator parallel to the AlGaN–GaN

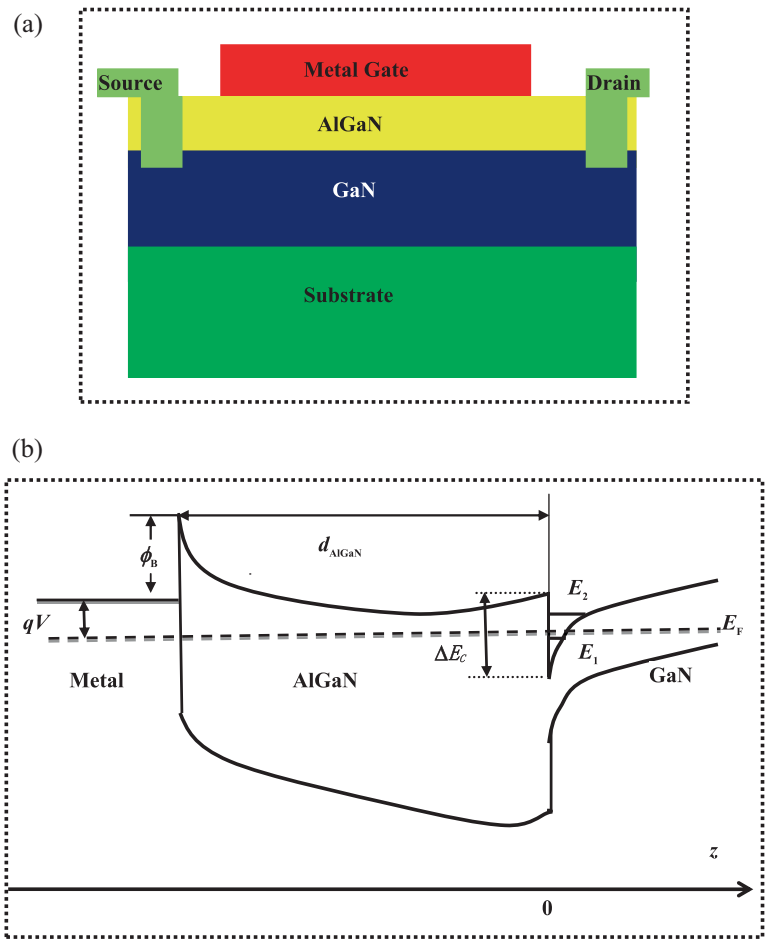

Figure 1. (**a**) Schematic cross-section and (**b**) the band diagram of the AlGaN/GaN HEMTs conventional structure.

interface and $\widehat{H}$ is the Hermitian operator), which represents the conservation of transverse electron momentum. Therefore, the solution $\xi(z) = \varphi(r,\theta)\psi(z)$ ($\varphi(r,\theta)$ and $\phi(z)$ are the wave functions which are parallel and perpendicular to the AlGaN–GaN interface), and $\phi(z)$ satisfies

$$\left[-\frac{\hbar^2}{2m_z(z)}\frac{\partial^2}{\partial z^2} + U(z)\right]\phi(z) = E_z(z)\phi(z). \tag{7}$$

The longitudinal electron energies in GaN, AlGaN and the metal gate of a GaN HEMT due to the transverse momentum conservation are

$$E_z^{\mathrm{GaN}} = E - \frac{\hbar^2 k_r^2}{2m^*_{\perp\text{-GaN}}}, \tag{8}$$

$$E_z^{\mathrm{AlGaN}} = E - \frac{\hbar^2 k_r^2}{2m^*_{\perp\text{-AlGaN}}}, \tag{9}$$

$$E_z^{\mathrm{G}} = E - \frac{\hbar^2 k_r^2}{2m^*_{\perp\text{-G}}}, \tag{10}$$

where k_r is the transverse wave vector, and $m^*_{\perp\text{-GaN}}$, $m^*_{\perp\text{-AlGaN}}$, $m^*_{\perp\text{-G}}$ are the effective transverse mass of the GaN, the AlGaN and the gate in a GaN HEMT, respectively. Equations (9) and (10) can be rewritten as

$$E_z^{\mathrm{AlGaN}} = E_z^{\mathrm{GaN}} + \frac{\hbar^2 k_r^2}{2m^*_{\perp\text{-GaN}}} - \frac{\hbar^2 k_r^2}{2m^*_{\perp\text{-AlGaN}}}, \tag{11}$$

$$E_z^{\mathrm{G}} = E_z^{\mathrm{GaN}} + \frac{\hbar^2 k_r^2}{2m^*_{\perp\text{-GaN}}} - \frac{\hbar^2 k_r^2}{2m^*_{\perp\text{-G}}}. \tag{12}$$

According to eqs (11) and (12), the Schrödinger equations in the GaN layer, the AlGaN layer, and the gate of a GaN HEMT are

$$\left[-\frac{\hbar^2}{2m^*_{\mathrm{GaN}\text{-}z}}\frac{\partial^2}{\partial z^2} + U(z)\right]\psi(z) = E_z^{\mathrm{GaN}}\psi(z), \tag{13}$$

$$\left[-\frac{\hbar^2}{2m^*_{\mathrm{AlGaN}\text{-}z}}\frac{\partial^2}{\partial z^2} + \left(U(z) - \left(1 - \frac{m^*_{\perp\text{-GaN}}}{m^*_{\perp\text{-AlGaN}}}\right)E_{\mathrm{tr}}\right)\right]\psi(z) = E_z^{\mathrm{GaN}}\psi(z), \tag{14}$$

$$\left[-\frac{\hbar^2}{2m^*_{\text{G-}z}}\frac{\partial^2}{\partial z^2} + \left(U(z) - \left(1 - \frac{m^*_{\perp\text{-GaN}}}{m^*_{\perp\text{-G}}}\right)E_{\text{tr}}\right)\right]\psi(z) = E_z^{\text{GaN}}\psi(z), \quad (15)$$

where $m^*_{\text{GaN-}z}$, $m^*_{\text{AlGaN-}z}$ and $m^*_{\text{G-}z}$ are the effective longitudinal mass of the GaN layer, the AlGaN layer and the gate in a GaN HEMT, respectively. Under the triangular quantum well approximation that $U(z) = qF_{\text{s\_GaN}}z$ ($F_{\text{s\_GaN}}$ is the normal surface electric field in the GaN layer whose direction is perpendicular to the AlGaN–GaN interface), the energy eigenvalues are [37–39]

$$E_{ij} = \left(\frac{\hbar^2}{2m^*_{\text{GaN-}z}}\right)^{1/3}\left[\frac{3\pi}{2}qF_{\text{s\_GaN}}\left(i + \frac{3}{4}\right)\right]^{2/3} \quad (i = 0, 1, 2, \ldots). \quad (16)$$

By solving the Poisson's equation under total depletion approximation [40,41], the sheet carrier density in the channel is

$$n_{\text{s}} = \frac{\varepsilon_{\text{AlGaN}}}{q(d_{\text{AlGaN}} + \Delta d)}\left[V_{\text{GS}} - \left(\frac{\phi_{\text{B}}}{q} - \frac{\Delta E_{\text{C}}}{q} - \frac{qN_{\text{D}}d^2_{\text{AlGaN}}}{2\varepsilon_{\text{AlGaN}}} - \frac{\sigma_{\text{AlGaN}}d_{\text{AlGaN}}}{\varepsilon_{\text{AlGaN}}}\right) - \frac{E_{\text{F}}}{q}\right], \quad (17)$$

where V_{GS} is the gate–source voltage, ϕ_{B} is the effective Schottky barrier height, ΔE_{C} is the conduction band offset between AlGaN and GaN, N_{D} is the doping density of the AlGaN layer, d_{AlGaN} is the thickness of the doped AlGaN layer, σ is the total amount of the sheet charge density induced by polarisation (including spontaneous polarisation, piezoelectric polarisation, etc.), $\varepsilon_{\text{AlGaN}}$ is the dielectric constant of the AlGaN layer and Δd is the average distance of the two-dimensional electron gas from the AlGaN–GaN interface [42]. One can note that $\Delta d = 2E_{0j}/(3qF_{\text{GaN\_eff}})$ [39] or it is typically 2–4 nm [43].

When a two-dimensional electron gas is formed at the AlGaN–GaN interface, the normal electric field at the two sides of the charge sheet by applying Gauss' law is

$$\varepsilon_{\text{gate}}F_{\text{s\_gate}}S + \varepsilon_{\text{GaN}}F_{\text{GaN}}S = \pm qn_{\text{s}}S, \quad (18)$$

where S is the unit area. When the electric flux through the gate–AlGaN interface is zero, it means that the electric field in the gate is zero, implying that the gate material is a metal or a conductor, and the normal surface electric field in the GaN layer equals $qn_{\text{s}}/\varepsilon_{\text{GaN}}$. When the electric flux through the gate–AlGaN interface is non-zero, e.g. the gate material is GaN, the normal surface electric field in the GaN layer equals $qn_{\text{s}}/2\varepsilon_{\text{GaN}}$, else let $R_{\text{E}}(qn_{\text{s}}/\varepsilon_{\text{GaN}})$. Here, R_{E} is the ratio of the electric flux through the AlGaN–GaN interface to total electric flux and thus, the normal surface electric field in the GaN side is

$$F_{\text{s\_GaN}} = \frac{R_{\text{E}}\varepsilon_{\text{AlGaN}}}{\varepsilon_{\text{GaN}}(d_{\text{AlGaN}} + \Delta d)}\times\left[V_{\text{GS}} - \left(\frac{\phi_{\text{B}}}{q} - \frac{\Delta E_{\text{C}}}{q} - \frac{qN_{\text{D}}d^2_{\text{AlGaN}}}{2\varepsilon_{\text{AlGaN}}} - \frac{\sigma_{\text{AlGaN}}d_{\text{AlGaN}}}{\varepsilon_{\text{AlGaN}}}\right) - \frac{E_{\text{F}}}{q}\right]. \quad (19)$$

$R_{\text{E}} = 1$ and $1/2$ represents the gate material being a metal (conductor) and GaN, respectively. The normal surface electric field in the AlGaN side is

$$F_{\text{s\_AlGaN}} = \frac{R_{\text{E}}}{(d_{\text{AlGaN}} + \Delta d)}\times\left[V_{\text{GS}} - \left(\frac{\phi_{\text{B}}}{q} - \frac{\Delta E_{\text{C}}}{q} - \frac{qN_{\text{D}}d^2}{2\varepsilon_{\text{AlGaN}}} - \frac{\sigma_{\text{AlGaN}}d_{\text{AlGaN}}}{\varepsilon_{\text{AlGaN}}}\right) - \frac{E_{\text{F}}}{q}\right]. \quad (20)$$

Equation (20) is the same as that in [39–41] when the gate is a metal. Due to the effective electron mass mismatch at the heterojunction interface, φ_{B} and ΔE_{C} seen by channel electrons will be

$$\phi_{\text{B}} + \left(1 - \frac{m^*_{\perp\text{-GaN}}}{m^*_{\perp\text{-G}}}\right)E_{\text{tr}} - \left(1 - \frac{m^*_{\perp\text{-GaN}}}{m^*_{\perp\text{-AlGaN}}}\right)E_{\text{tr}}$$

and

$$\Delta E_{\text{C}} - \left(1 - \frac{m^*_{\perp\text{-GaN}}}{m^*_{\perp\text{-AlGaN}}}\right)E_{\text{tr}}.$$

Therefore, the normal surface electric field in the channel is

$$F_{\text{sc\_GaN}} = F_{\text{s\_GaN}} + \frac{R_{\text{E}}}{d_{\text{AlGaN}} + \Delta d}\times\left(1 - \frac{m^*_{\perp\text{-GaN}}}{m^*_{\perp\text{-G}}}\right)\frac{E_{\text{tr}}}{q}. \quad (21)$$

Using a first-order Taylor series approximation, the quantised energy levels after considering the quantum

coupling are

$$E_{ij-c} = E_{ij} + \frac{2}{3F_{\text{s\_GaN}}}\frac{1}{d_{\text{AlGaN}} + \Delta d}\left(1 - \frac{m^*_{\perp\text{-GaN}}}{m^*_{\perp\text{-G}}}\right) \times \left(\frac{\hbar^2}{2m^*_{\text{GaN-}z}}\left[\frac{3\pi}{2}q\left(i + \frac{3}{4}\right)\right]^2\right)^{1/3} \frac{E_{\text{tr}}}{q} \quad i = 0, 1, 2, \ldots. \tag{22}$$

Under the assumption that only the first two quantum states are occupied by channel electrons, the electron density in the channel is [44]

$$n_{\text{inv}} = k_{\text{B}}T_{\text{L}}\frac{m^*_{\perp\text{-GaN}}}{\pi\hbar^2} \times \ln\left[\left(1 + \mathrm{e}^{(E_{\text{F}} - E_{0j})/k_{\text{B}}T_{\text{L}}}\right) \times \left(1 + \mathrm{e}^{(E_{\text{F}} - E_{1j})/k_{\text{B}}T_{\text{L}}}\right)\right], \tag{23}$$

where $m^*_{\perp\text{-GaN}}$ is the effective transverse electron mass of GaN and E_{F} is the Fermi level. Thus, the source–drain current is

$$\begin{aligned} I_{\text{D}} &= \frac{Z}{L}\int_0^L Q_n(x)v_{\text{d}}(x)\mathrm{d}x \\ &= \frac{Z\mu q}{L}\frac{k_{\text{B}}T_{\text{L}}m^*_{\perp\text{-GaN}}}{\pi\hbar^2} \times \ln[(1+\mathrm{e}^{(E_{\text{F}} - E_{0j})/k_{\text{B}}T_{\text{L}}}) \times (1+\mathrm{e}^{(E_{\text{F}} - E_{1j})/k_{\text{B}}T_{\text{L}}})]V_{\text{DS}} \\ &= Zq\frac{k_{\text{B}}T_{\text{L}}m^*_{\perp\text{-GaN}}}{\pi\hbar^2} \times \ln[(1+\mathrm{e}^{(E_{\text{F}} - E_{0j})/k_{\text{B}}T_{\text{L}}})(1+\mathrm{e}^{(E_{\text{F}} - E_{1j})/k_{\text{B}}T_{\text{L}}})]v_{\text{d}}, \end{aligned} \tag{24}$$

where V_{DS} is the source–drain voltage, v_{d} is the average drift velocity of channel electrons, Q_n is the channel electron density and Z is the channel width. For simplicity, we assume that $\left(E_{\text{F}} - E_{0j}\right) \gg k_{\text{B}}T_{\text{L}}$ and $\left(E_{\text{F}} - E_{1j}\right) \gg k_{\text{B}}T_{\text{L}}$. The source–drain current without considering the quantum coupling is

$$\begin{aligned} I_{\text{D}} &= Z\mu q\frac{m^*_{\perp\text{-GaN}}}{\pi\hbar^2} \times \left[2E_{\text{F}} - \left(\frac{225(q\pi\hbar)^2}{32m^*_{\text{GaN-}z}}\right)^{1/3}[F_{\text{s}}]^{2/3}\right]F_{\text{ch}} \\ &= Zqv_{\text{d}}\frac{m^*_{\perp\text{-GaN}}}{\pi\hbar^2} \times \left[2E_{\text{F}} - \left(\frac{225(q\pi\hbar)^2}{32m^*_{\text{GaN-}z}}\right)^{1/3}[F_{\text{s}}]^{2/3}\right]. \end{aligned} \tag{25}$$

By using a first-order Taylor series expansion, the source–drain current after considering the quantum coupling is

$$\begin{aligned} I_{\text{D\_C}} &\approx Zv_{\text{d}}q\frac{m^*_{\perp\text{-GaN}}}{\pi\hbar^2} \times \left[2E_{\text{F}} - \left(\frac{225(q\pi\hbar)^2}{32m^*_{\text{GaN-}z}}\right)^{1/3}(F_{\text{s}})^{2/3} \times \left(1 + \frac{2}{3}\frac{\varepsilon_{\text{AlGaN}}}{\varepsilon_{\text{GaN}}(d_{\text{AlGaN}} + \Delta d)} \left(1 - \frac{m^*_{\perp\text{-GaN}}}{m^*_{\perp\text{-AlGaN}}}\right)\frac{E_{\text{tr}}}{qF_{\text{s}}}\right)\right] \\ &= I_{\text{D}} - \frac{Z(v_{\text{d}})^2}{(F_{\text{s}})^{1/3}}\frac{2m^*_{\perp\text{-GaN}}\varepsilon_{\text{AlGaN}}q\tau_{\text{e}}F_{\text{ch}}}{3\pi\hbar^2\varepsilon_{\text{GaN}}(d_{\text{AlGaN}} + \Delta d)} \times \left(\frac{225(q\pi\hbar)^2}{32m^*_{\text{GaN-}z}}\right)^{1/3}\left(1 - \frac{m^*_{\perp\text{-GaN}}}{m^*_{\perp\text{-AlGaN}}}\right). \end{aligned} \tag{26}$$

Equation (26) clearly illustrates that the quantum coupling changes the source–drain current in GaN HEMTs.

3. Results and discussion

The values used in this paper are: The Schottky barrier height = 0.7 eV for the metal–GaN contact [45], relative dielectric constant = 9.5 for GaN [46] and 9.2 for $Al_{0.3}Ga_{0.7}N$ [47], band gap = 3.4 eV for GaN [48] and 4.24 eV for $Al_{0.3}Ga_{0.7}N$ [49], electron mobility = 1300 $\text{cm}^2/\text{V/s}$ in GaN [50], the transversal mass = $0.186m_0$, the longitudinal mass = $0.209m_0$ for electrons in GaN [51], the longitudinal electron mass = $0.245m_0$ for $Al_{0.3}Ga_{0.7}N$ calculated by a linear increase of the effective mass with increasing Al content [52], the conduction band offset between $Al_{0.3}Ga_{0.7}N$ and GaN = 0.65 eV [53], the polarisation electron concentration = $2 \times 10^{-6}\,\text{C/cm}^2$ for GaN and $4.69 \times 10^{-6}\,\text{C/cm}^2$ for $Al_{0.3}Ga_{0.7}N$ [54]. A 300 nm thick GaN, channel width of 1 μm, channel length of 1 μm and 4 nm thick $Al_{0.3}Ga_{0.7}N$ have been used in the numerical solutions to the coupled Schrödinger and Poisson equations.

According to eq. (5), the transverse electron energy is $q\mu_{\text{e}}\tau_{\text{e}}(F_{\text{ch}})^2 + k_{\text{B}}T_{\text{L}}$. Thus, the total electron energy is $q\mu_{\text{e}}\tau_{\text{e}}(F_{\text{ch}})^2 + (3/2)k_{\text{B}}T_{\text{L}}$, which means that the effective electron temperature $T_{\text{e}} = ((q\mu_{\text{e}}\tau_{\text{e}}(F_{\text{ch}})^2)/(3/2)k_{\text{B}}) + T_{\text{L}}$.

Figure 2 clearly demonstrates that the quantised levels in the channel of a GaN HEMT calculated by the proposed model agree well with those by the numerical solutions. The difference between the results could have

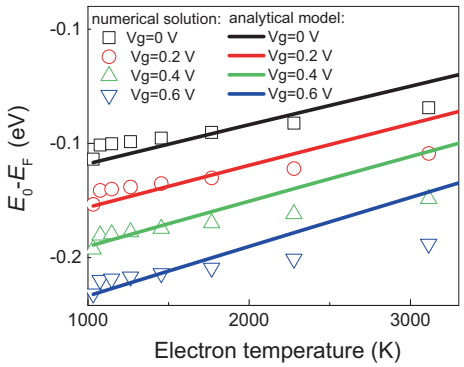

Figure 2. The comparison of the first quantised energy levels as a function of electron temperature calculated by the proposed analytical model and the numerical calculations.

been originated from the triangular potential approximation for the two-dimensional gas. Note that $E_{ij-c} \propto E_{\mathrm{tr}}$ according to eq. (22), which means that the quantised energy levels increase linearly with the transverse electron energy. All values of adj. R^2 in linear fitting in figure 2 are found to be larger than 0.995. It means that both models can be used to describe the quantised level dependencies on the electron temperature because Adj. R^2 is the adjusted coefficient of determination in statistics and it tells one that what per cent of the total variability is accounted for by one model. When the transversal electron mass of GaN is $0.186m_0$, the electron temperature in the plane of 1159, 2318 and 3478 K corresponds to the average electron drift velocity of 3.5×10^5, 5.5×10^5 and 6.8×10^5 m/s, respectively. Peak transient drift velocities around 7.5×10^5 m/s, the average drift velocities around 4.3×10^5 m/s [56] and the peak electron transient velocity of 7.25×10^5 m/s [57] for GaN at room temperature were reported. It implies that the electron drift velocities used in this paper are reasonable.

Using the momentum and energy relaxation time and effective mass of AlGaN/GaN transistors under various direct-current biases reported in Table III in [55], we can calculate the electron kinetic energy at different channel electric fields. Additionally, the kinetic electron energy ($E_k = q\mu_e\tau_e(F_{\mathrm{ch}})^2$) due to the channel electric field has been found to increase exponentially with the channel electric field. For an exponential fitting of the data in Table III in [55], we obtain

$$E_k = k_{\mathrm{B}}(443.3 + 45.7 * \exp(F_{\mathrm{ch}}/20.3)).$$

The unit of temperature is K and the unit of channel field is kV/cm. The value of Adj. R^2 in the exponential fitting is 0.99997. It means that the fitting process is successful. Thus, such an exponential relation has been used to calculate the transverse electron energy in the data of figures 3–10 obtained in the calculations.

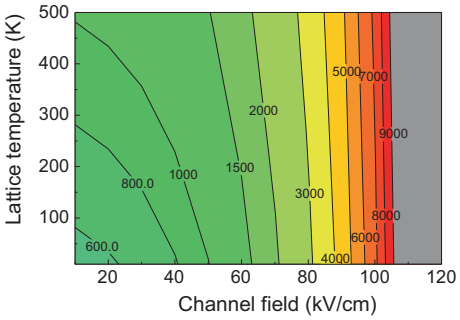

Figure 3. Contour of the electron temperature in GaN HEMTs between the channel electric field and the lattice temperature.

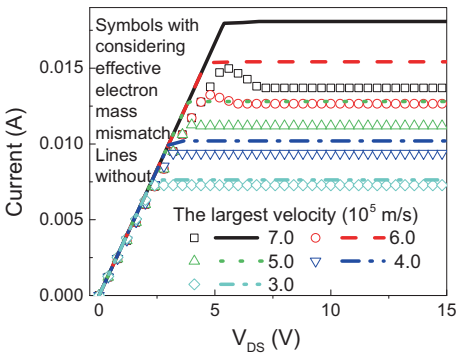

Figure 4. The source–drain current as a function of source–drain voltage with and without considering the quantum coupling.

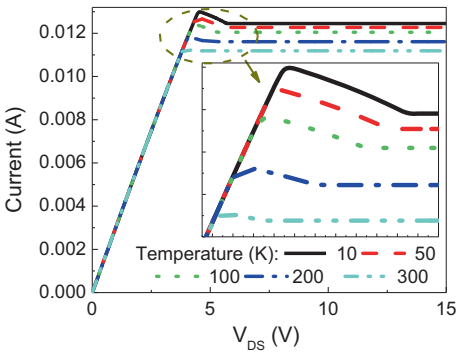

Figure 5. The source–drain current as a function of the source–drain voltage at the largest electron drift velocity of 5×10^5 m/s for different lattice temperatures.

In the data of figures 3–10 obtained in the calculations, for simplicity and ease of understanding, we assume constant electron mobility and a saturation drift velocity.

Figure 3 depicts the contour of the electron temperature between the lattice temperature and the channel electric field. It is clearly seen from this figure that a medium channel electric field at a given lattice temperature will lead to a very large electron temperature in the channel. This figure illustrates that channel electrons can get large energy from the channel electric

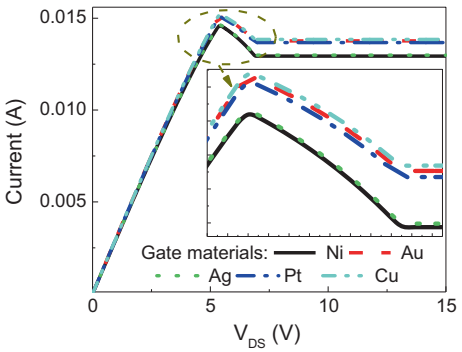

Figure 6. The source–drain current as a function of the source–drain voltage at the largest electron drift velocity of 7×10^5 m/s for different gate metals.

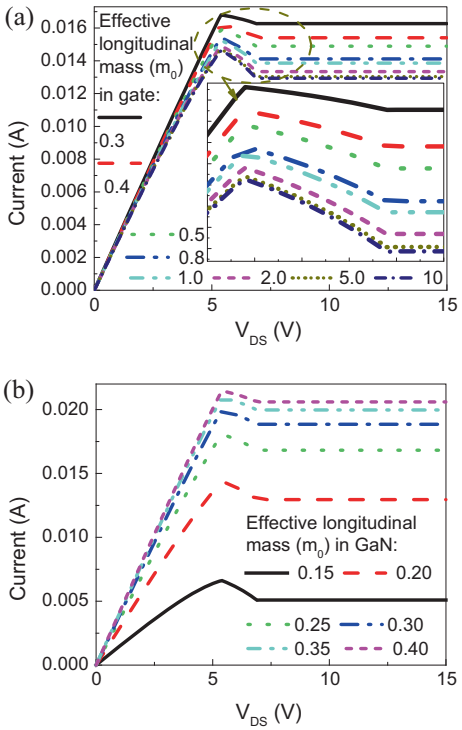

Figure 7. The source–drain current as a function of the source–drain voltage at the largest electron drift velocity of 7×10^5 m/s for different effective longitudinal electron mass of (**a**) the gate and (**b**) GaN.

field in GaN HEMTs. Consequently, the barrier height seen by channel electrons with a very large electron temperature will be largely reduced. Such a high electron temperature via the quantum coupling between the longitudinal and transverse components of the three-dimensional motions of channel electrons will affect the quantisation in GaN transistors, redistribute the channel electron density and finally change the performance of GaN transistors.

Figure 4 gives a comparison of the source–drain current calculated by the proposed model with and

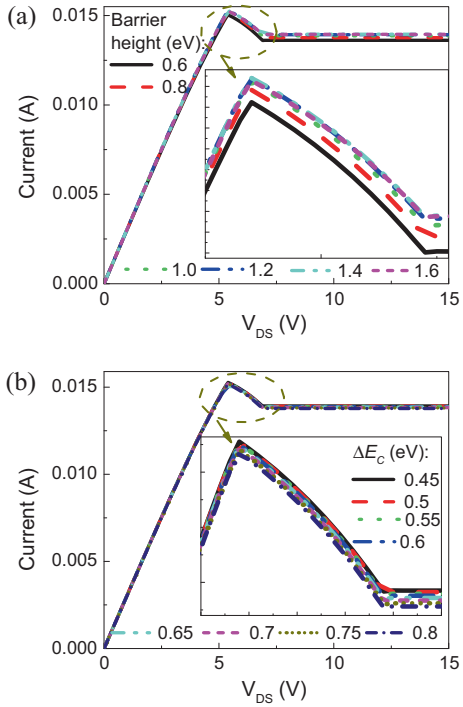

Figure 8. The source–drain current as a function of the source–drain voltage at the largest electron drift velocity of 7×10^5 m/s for (**a**) different Schottky barrier height and (**b**) conduction band offset between $Al_{0.3}Ga_{0.7}N$ and GaN.

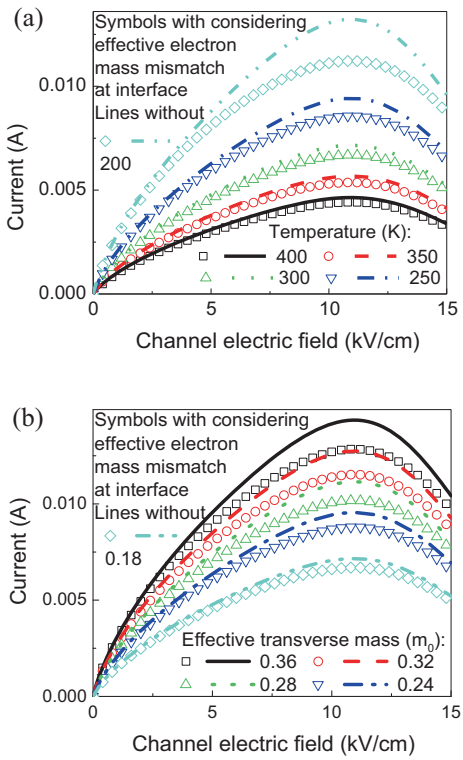

Figure 9. The source–drain current as a function of source–drain voltage when the gate material is Au for (**a**) different lattice temperatures and (**b**) different effective transverse electron mass of GaN.

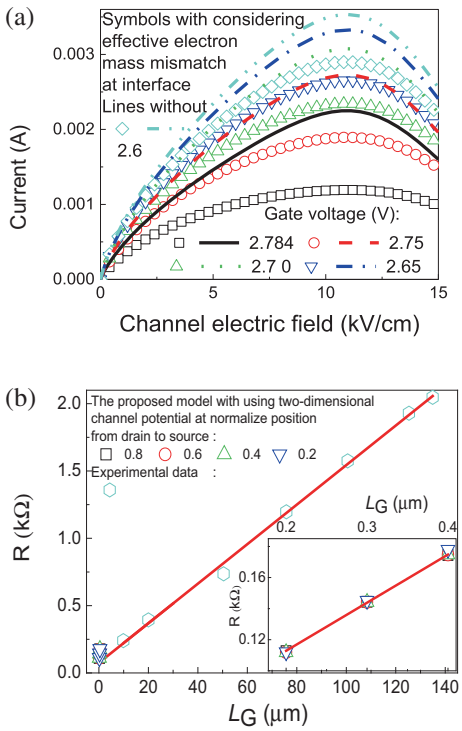

Figure 10. (**a**) The source–drain current as a function of source–drain voltage and (**b**) the channel resistance as a function of the gate length of GaN HEMT.

without considering the quantum coupling. The current collapse can be observed in this figure when the electron energy = 0.19 eV or the electron temperature = 1771 K or the average electron drift velocity = 6×10^5 m/s with an effective electron mass of $0.186m_0$ for GaN or 6.1×10^5 m/s with $0.18m_0$ or 5.3×10^5 m/s with $0.25m_0$ or 4.7×10^5 m/s with $0.3m_0$ or 4.3×10^5 m/s with $0.36m_0$. More pronounced current collapse can be observed when the average drift velocity = 7×10^5 m/s or the electron energy = 0.259 eV or the electron temperature = 2303 K or the average electron drift velocity = 7×10^5 m/s with an effective electron mass of $0.186m_0$ for GaN. Note that the electron temperature is much larger than 2000 K [58] and the maximum electron temperature can be higher than 6000 K [59] in GaN transistors. Thus, current collapse caused by the quantum coupling can be easily observed in GaN HEMTs due to such high electron temperature. Note that the relative decrease in the source–drain current caused by the quantum coupling = 4.6% when the electron temperature = 1771 K. Figure 4 proves that the quantum coupling at the AlGaN–GaN interface and electrons in the channel with large enough energy are the possible physical origin of the current collapse in GaN HEMTs. When the transverse energy in the channel is larger than the conduction band offset between AlGaN and GaN, such high-energy hot electrons will not be in quantised states of the channel, thus current collapse can disappear.

The saturation velocity in GaN was modelled by

$$v_{\text{sat}} = \frac{v_{\text{sat300}}}{(1 - A_n) + A_n(T_{\text{L}}/300)}$$

with $A_n = 0.25$ [60]. The saturation velocity of 3×10^5 m/s was chosen in the calculations [61]. Figure 5 clearly shows that the current collapse in GaN HEMTs is less obvious with the increased lattice temperature. Such a temperature-dependent current collapse agrees well with the conclusions observed in experiments that increased temperature can partially eliminate the current collapse in GaN HEMTs [62,63].

Figure 6 shows how the gate materials impact the current collapse. Schottky barrier height of Cu, Ni, Ag, Pt and Au on GaN as 0.97, 1.13, 0.66, 1.16 and 0.98 eV [64] and the effective masses in Cu, Ni, Ag, Pt and Au of $1.01m_0$, $28m_0$, $0.99m_0$, $13m_0$ and $1.10m_0$ [65] have been used. Figure 6 clearly shows that the current collapse will be affected by using different gate metal in GaN HEMTs. It agrees well with the experimental observations in GaN HEMTs [66].

Figure 7a shows how the effective longitudinal electron mass of the gate affects the current collapse in GaN HEMTs. It is clearly shown in this figure that the current collapse in GaN HEMTs is dependent on the effective longitudinal electron mass of the gate. Figure 7b shows how the effective longitudinal electron mass of GaN affects the current collapse in GaN HEMTs. This figure clearly illustrates that when the effective longitudinal electron mass of GaN is less, the current collapse in GaN HEMTs is more pronounced .

Figure 8a shows how the Schottky barrier height affects the source–drain current in GaN HEMTs. Figure 8b shows how the conduction band offsets between AlGaN and GaN affects the source–drain current in GaN HEMTs. The current collapse in GaN HEMTs is very weakly dependent on the Schottky barrier height and the conduction band offset can be easily observed in figure 8.

In the above discussion, we neglect the velocity–field relation for better observation of the effects of the effective electron mismatch at the heterojunction interface and hot electrons in the channel on the source–drain current in GaN HEMTs. An analytical relation between the electron mobility and the channel electric field for the $Al_{0.3}Ga_{0.7}N$/GaN structure is [67]

$$\mu_{\text{e}} = \frac{\mu_0 + v((F_{\text{ch}})^{\alpha-1}/(F_{\text{c}})^{\alpha})}{1 + \xi(F_{\text{ch}}/F_{\text{c}})^{\beta} + (F_{\text{ch}}/F_{\text{c}})^{\alpha}}, \tag{27}$$

where $\alpha = 7.057$, $\beta = 0.486$, $\xi = 3.6524$ and $F_{\text{c}} = 122.3389$ at room temperature. When the

transverse energy in the channel of GaN HEMTs is constant, the average drift velocity will be determined by the transverse electron mass and the lattice temperature according to eq. (5). Note that the transverse electron mass of GaN reported in the literature has different values. For example, it was reported as $0.228m_0$ in [68], 0.18–$29m_0$ in [69] and 0.22–$0.39m_0$ in [70]. The transverse electron mass of $0.36m_0$ is chosen in the calculations of figure 9a. It can be clearly seen from figure 9a that the source–drain current in GaN HEMTs decreases with the source–drain voltage when it is large enough. Such a decrease in source–drain current in GaN HEMTs comes from the velocity–field relation. Figure 9a clearly shows that the quantum coupling is neglected for high lattice temperatures, whereas it should be seriously considered for low lattice temperatures. Figure 9b shows how the transverse electron mass affects the source–drain current in GaN HEMTs with and without considering the quantum coupling. Obviously, with a larger transverse electron mass of GaN, a more pronounced decrease in the source–drain current occurs in GaN HEMTs.

According to eq. (5), the average transverse energy is also affected by the energy relaxation time. The energy relaxation time can be described as $\tau_e = (E - E_0)/qvF_{ch}$ (E_0 is the equilibrium energy at zero applied channel field) [71]. Note that $E - E_0 = (1/2)m^*_{\perp\text{-GaN}}v^2$, which means that $\tau_e = (m^*_{\perp\text{-GaN}}v)/2qF_{ch}$. Thus, the effects of electron energy relaxation time on the source–drain current in GaN HEMTs are similar to those considering the velocity–field relation because the velocity–field relation implies such a dependent relation.

Figure 10a shows how the gate voltage affects the source–drain current in GaN HEMTs. The lines represent those that have been calculated without considering the quantum coupling but including the velocity–field relation (eq. (27)). Such a velocity–field relation always decreases the source–drain current in the saturation region, which is clearly shown in figure 10a. This conclusion is contrary to the experimental observation that the current collapse varies with gate voltage [72]. However, figure 10a clearly demonstrates that the current collapse predicted by the proposed mode agrees well with the experiments in GaN HEMTs [72]. Additionally, the current reduction is found to be more pronounced for shorter gate length in GaN HEMTs [73], which can also be physically explained by using the proposed model. A new term related to the drain voltage for a two-dimensional channel potential distribution, which is $-(\varepsilon_{AlGaN}/(q(d_{AlGaN} + \Delta d)))V_{ch}$, is introduced in eqs (17), (19) and (20). Therefore, the normal electric field is affected by the drain voltage and affects the current collapse in GaN HEMTs according to eq. (26). Note that the channel potential in GaN HEMTs can be directly affected by the gate length (e.g. [74]), and thus leads to a gate length-dependent current collapse. Figure 10b compares the resistances obtained from the experimental data (open hexagons) in [73] with those predicted by the proposed model (open squares, circles, triangles and inverted triangles) by using the two-dimensional channel potential at the normalised position of 0.2, 0.4, 0.6 and 0.8 obtained in [74]. This figure clearly demonstrates that the gate length dependencies of resistance predicted by the proposed model agree well with the experimental data.

The two-step field-plate structure can affect the current collapse in GaN HEMTs because it can relax the electric-field concentration [75]. It can be easily explained by using the proposed model because the channel electric field determines the transverse energy in GaN HEMTs according to eq. (5), which can affect the quantised energy level according to eq. (22), redistribute the channel electron density and change the surface potential. Thus, the surface electric field (surface potential) in the channel can affect the current collapse in GaN HEMTs according to eq. (26). The current collapse in GaN HEMTs is suppressed by passivation, which is caused by the surface potential modulation but the exact passivation mechanism still remains a matter of debate [76]. Note that the surface potential modulation will change the normal surface electric field in the channel, and thus the alleviation in the current collapse in GaN HEMTs can be easily explained by using the proposed model because the normal surface electric field in the channel affects the source–drain current according to eq. (26). In the proposed model, the effects of physical parameters on the current collapse in GaN HEMTs can be easily analysed, and thus it can be alleviated through proper optimisation of growth parameters and structure parameters. For example, some researchers believe that it is possible to suppress the current collapse in GaN HEMTs with p-GaN gate [77], which can be physically explained because the quantum coupling of hot electrons in the channel of GaN HEMTs is least when the effective-mass mismatch is least according to eqs (13)–(15), (21) and (24).

The energy and momentum relaxation rates are affected by electron–phonon interaction, hot phonons, plasmons, intervalley scattering, polaritons, hole–optical–phonon interaction, carrier–carrier interactions, acoustic phonons, charged impurities and alloy scattering [78]. Therefore, the current collapse in GaN HEMTs will be strongly affected by whatever can largely impact the energy and momentum relaxation rates such as phonon, intervalley scattering, injection in traps, charged impurities, etc., according to eq. (5). Details on how the phonon affects the effective energy

relaxation time and momentum relaxation time can be found in [79–81].

4. Conclusions

To summarise, quantum coupling among the motions of the channel electrons in the GaN HEMTs on the current collapse has been theoretically investigated and physically modelled. Based on the combination of the energy (momentum) conservation equations and the three-dimensional Schrödinger equations in the regions of the GaN layer, the AlGaN layer and the gate of the GaN HEMT, an analytical–physical model has been built to describe the current collapse observed in the experiments. The electrothermal effects or the energy relaxation of the channel electrons in the GaN HEMTs can result in very high electron temperature, thereby causing a reduction in the effective barrier height seen by the channel electrons. Thus, it redistributes the two-dimensional channel electron density. Further, it can decrease the source–drain current because rising quantised levels lead to a decrease in the conduction electron density in the channel of GaN HEMTs. The proposed model agrees well with the experimental observation in the literature. Hot-electron effects can lead to a very high electron temperature of the two-dimensional electrons in GaN HEMTs. The effective electron mass mismatch at the interface can cause the occurrence of the current collapse when the electron temperature is large enough. Effects of physical parameters such as gate metals, temperature, electric field, gate length, effective electron mass, passivation and the field-plate structure on the current collapse in GaN HEMTs have been investigated in detail. It reveals the correlation between the physical parameters of a GaN HEMT and the current collapse. Thus, the current collapse in GaN HEMTs can be alleviated by optimising device parameters. Through this study, it is evident that the quantum coupling and hot-electron effects should be seriously considered in the characterisation and modelling of GaN HEMTs or other HEMTs. Further physical understanding of the combination of the electrothermal effects and the quantum coupling among the motions of the channel electrons in the GaN HEMTs is of great importance for the design of device structure and its applications.

Acknowledgements

The author acknowledges the financial support from the National Natural Science Foundation of China under Grant No. 61774014 and the Central Universities under Grant No. 06500010.

References

[1] J A Mittereder, S C Binari, P B Klein, J A Roussos, D S Katzer, D F Storm, D D Koleske, A E Wickenden and R L Henry, *Appl. Phys. Lett.* **83**, 1650 (2003)
[2] M J Uren, J Möreke and M Kuball, *IEEE Trans. Electron. Dev.* **59**, 3327 (2012)
[3] E Zanoni, G Meneghesso, G Verzellesi, F Danesin, M Meneghini, F Rampazzo, A Tazzoli and F Zanon, *IEDM Technical Digest* (Washington, USA, 1997) pp. 381–384
[4] C Lee, H Tserng, L Witkowski, P Saunier, S Guo, B Albert, R Birkhahn and G Munns, *Electron. Lett.* **40**, 1147 (2004)
[5] M Iqbal, P S Ko and S D Kim, *Curr. Appl. Phys.* **14**, 1099 (2014)
[6] T Mizutani, Y Ohno, M Akita, S Kishimoto and K Maezawa, *IEEE Trans. Electron. Dev.* **50**, 2015 (2003)
[7] M J Anand, G I Ng, S Vicknesh, S Arulkumaran and K Ranjan, *Phys. Status Solidi C* **10**, 1421 (2013)
[8] D Jin, J Joh, S Krishnan, N Tipirneni, S Pendharkar and J A del Alamo, *IEDM Technical Digest* (Washington, USA, 2013) pp. 148–151
[9] B M Green, K K Chu, E M Chumbes, J A Smart, J R Shealy and L F Eastman, *IEEE Electron. Dev. Lett.* **21**, 268 (2000)
[10] A P Edwards, J A Mittereder, S C Binari, D S Katzer, D F Storm and J A Roussos, *IEEE Electron. Dev. Lett.* **26**, 225 (2005)
[11] S M Razavi, S H Zahiri and S E Hosseini, *Pramana – J. Phys.* **88**: 85 (2017)
[12] R Swain, K Jena and T R Lenka, *Pramana – J. Phys.* **88**: 3 (2017)
[13] K Jena, R Swain and T R Lenka, *Pramana – J. Phys.* **85**, 1221 (2015)
[14] J Joh and J A Del Alamo, *IEEE Electron. Dev. Lett.* **29**, 287 (2008)
[15] X D Wang, W D Hu, X S Chen and W Lu, *IEEE Trans. Electron. Dev.* **59**, 1393 (2012)
[16] G Meneghesso, G Verzellesi, F Danesin, F Rampazzo, F Zanon, A Tazzoli, M Meneghini and E Zanoni, *IEEE Trans. Device Mater. Reliab.* **8**, 332 (2008)
[17] K Fushinobu and T Hatakeyama, *Trans. Jpn. Inst. Electron. Packag.* **4**, 31 (2011)
[18] H Rao and G Bosman, *Solid State Electron.* **79**, 11 (2013)
[19] L F Mao, *Pramana – J. Phys.* **72**, 407 (2009)
[20] L F Mao, H Ning and J Y Wang, *PLoS One* **10**, e0128438 (2015)
[21] L F Mao, H Ning, Z L Huo and J Y Wang, *Sci. Rep.* **5**, 18307 (2015)
[22] L F Mao, H Ning, Z Lu and G Wang, *Sci. Rep.* **6**, 24777 (2016)
[23] L F Mao, *ETRI J.* **39**, 284 (2017)
[24] L F Mao, J Wang, L Li, H Ning and C Hu, *Carbon* **119**, 446 (2017)

[25] I Hwang, J Kim, H-S Choi, J Oh, J-K Shin and U-I Chung, *IEEE Electron. Dev. Lett.* **34**, 1494 (2013)
[26] L F Mao, *Appl. Phys. Lett.* **90**, 183511 (2007)
[27] L F Mao, *Appl. Phys. Lett.* **91**, 123519 (2007)
[28] L F Mao, *IEEE Electron. Dev. Lett.* **28**, 161 (2007)
[29] L F Mao, *IEEE Trans. Electron. Dev.* **55**, 782 (2008)
[30] L F Mao, *Solid State Electron.* **52**, 186 (2008)
[31] L F Mao, *ETRI J.* **32**, 68 (2010)
[32] R G Southwick, J Reed, C Buu, H Bui, R Butler, G Bersuker and W B Knowlton, *IEEE International Integrated Reliability Workshop* (S. Lake Tahoe, USA, 2008) pp. 48–54
[33] W D Hu, X S Chen, Z J Quan, C S Xia, W Lu and P D Ye, *J. Appl. Phys.* **100**, 074501 (2006)
[34] D Bisi, M Meneghini, C de Santi, A Chini, M Dammann, P Brückner, M Mikulla, G Meneghesso and E Zanoni, *IEEE Trans. Electron. Dev.* **60**, 3166 (2013)
[35] S Kaneko, M Kuroda, M Yanagihara, A Ikoshi, H Okita, T Morita, K Tanaka, M Hikita, Y Uemoto, S Takahashi and T Ueda, *Proceedings of IEEE 27th International Symposium on Power Semiconductor Devices and ICs* (Hong Kong, China, 2015) pp. 41–44
[36] H Jiang, J M Hinckley and J Singh, *IEEE J. Quant. Electron.* **33**, 1779 (1997)
[37] C Moglestue, *J. Appl. Phys.* **59**, 3175 (1986)
[38] F Stern, *Phys. Rev. B* **5**, 4891 (1972)
[39] S Rabbaa and J Stiens, *J. Phys. D* **44**, 325103 (2011)
[40] W Liu, *Fundamentals of III–V devices—HBTs, MESFETs, and HFETs/HEMTs* (Wiley, Hoboken, NJ, 1999)
[41] A Kranti, S Haldar and R S Gupta, *Solid State Electron.* **46**, 621 (2002)
[42] M A Huque, S A Eliza, T Rahman, H F Huq and S K Islam, *Solid State Electron.* **53**, 134 (2009)
[43] A Loghmany and P Valizadeh, *J. Phys. D* **44**, 125102 (2011)
[44] S Khandelwal, Y S Chauhan and T A Fjeldly, *IEEE Trans. Electron. Dev.* **59**, 2856 (2012)
[45] T Sawada, Y Ito, K Imai, K Suzuki, H Tomozawa and S Sakai, *Appl. Surf. Sci.* **159**, 449 (2000)
[46] A S Barker and M Ilegems, *Phys. Rev. B* **7**, 743 (1973)
[47] D Wang, W D Hu, X S Chen, J T Xu, X Y Li and W Lu, *Opt. Quant. Electron.* **42**, 755 (2011)
[48] Y I Alivov, E V Kalinina, A E Cherenkov, D C Look, B M Ataev, A K Omaev, M V Chukichev and D M Bagnall, *Appl. Phys. Lett.* **83**, 4719 (2003)
[49] T R Lenka and A K Panda, *Pramana – J. Phys.* **79**, 151 (2012)
[50] T H Yu and K F Brennan, *J. Appl. Phys.* **89**, 3827 (2001)
[51] P Rinke, M Winkelnkemper, A Qteish, D Bimberg, J Neugebauer and M Scheffler, *Phys. Rev. B* **77**, 075202 (2008)
[52] S Schöche, P Kühne, T Hofmann, M Schubert, D Nilsson, A Kakanakova-Georgieva, E Janzén and V Darakchieva, *Appl. Phys. Lett.* **103**, 212107 (2013)
[53] D J As, A Zado, Q Y Wei, T Li, J Y Huang and F A Ponce, *Jpn. J. Appl. Phys.* **52**, 08JN04 (2013)
[54] X Yi, H Sun, Y Xiao, H Yang and K Fu, *OSA-IEEE-COS.* (Guangzhou, China, 2010) pp. 1–4
[55] Y R Wu, J M Hinckley and J Singh, *J. Electron. Mater.* **37**, 578 (2008)
[56] D Pavlidis, *European Galliun Arsenide Related III–V Compound Application Symposium* (Amsterdam, Netherlands, 2004) pp. 551–554
[57] M Wraback, H Shen, J C Carrano, C J Collins, J C Campbell, R D Dupuis, M J Schurman and I T Ferguson, *Appl. Phys. Lett.* **79**, 1303 (2001)
[58] C H Oxley, M J Uren, A Coates and D G Hayes, *IEEE Trans. Electron. Dev.* **53**, 565 (2006)
[59] B Padmanabhan, D Vasileska and S M Goodnick, *J. Comput. Electron.* **11**, 129 (2012)
[60] R Quay, *Analysis and simulation of high electron mobility transistors*, Ph.D. dissertation (Technische Universität Wien, 2001)
[61] S Yagi, S Hirata, Y Sumida, A Nakajima, H Kawai, E M Sankara Narayanan, *Proceedings of the SSDM* (Nagoya, Japan, 2011) pp. 570–571
[62] C Zhang, M Wang, B Xie, C P Wen, J Wang, Y Hao, W Wu, K J Chen and B Shen, *IEEE Trans. Electron. Dev.* **62**, 2475 (2015)
[63] C S Oh, C J Youn, G M Yang, K Y Lim and J W Yang, *Appl. Phys. Lett.* **86**, 012106 (2005)
[64] A C Schmitz, A T Ping, M Asif Khan, Q Chen, J W Yang and I Adesida, *J. Electron. Mater.* **27**, 255 (1998)
[65] S O Kasap, *Principles of electronic materials and devices*, 3rd edn (McGraw-Hill, New York, 2005)
[66] T Kawanago, K Kakushima, Y Kataoka, A Nishiyama, N Sugii, H Wakabayashi, K Tsutsui, K Natori and H Iwai, *ESSDERC* (Bucharest, Romania, 2013) pp. 107–110
[67] T H Yu and K F Brennan, *J. Appl. Phys.* **91**, 3730 (2002)
[68] A Kasic, M Schubert, S Einfeldt, D Hommel and T E Tiwald, *Phys. Rev. B* **62**, 7365 (2000)
[69] C E Dreyer, A Janotti and C G Van de Walle, *Appl. Phys. Lett.* **102**, 142105 (2013)
[70] T Hofmann, P Kühne, S Schöche, J-T Chen, U Forsberg, E Janzén, N Ben Sedrine, C M Herzinger, J A Woollam, M Schubert and V Darakchieva, *Appl. Phys. Lett.* **101**, 192102 (2012)
[71] B E Foutz, S K O'Leary, M S Shur and L F Eastman, *J. Appl. Phys.* **85**, 7727 (1999)
[72] G Simin, A Koudymov, A Tarakji, X Hu, J Yang and M Asif Khan, *Appl. Phys. Lett.* **79**, 2651 (2001)
[73] K Itagaki, N Kobayashi and K Horio, *Phys. Status. Solidi C* **4**, 2666 (2007)
[74] T Ahmed, M T A Khan and M S Islam, *IEEE International Conference on Devices, Circuits and Systems* (Coimbatore, India, 2012) pp. 226–229
[75] W Saito, Y Kakiuchi, T Nitta, Y Saito, T Noda, H Fujimoto, A Yoshioka, T Ohno and M Yamaguchi, *IEEE Electron. Dev. Lett.* **31**, 659 (2010)
[76] D W DiSanto, H F Sun and C R Bolognesi, *Appl. Phys. Lett.* **88**, 013504 (2006)
[77] M Meneghini, O Hilt, J Wuerfl and G Meneghesso, *Energies* **10**, 153 (2017)

[78] B K Ridley, *Rep. Prog. Phys.* **54**, 169 (2002)
[79] N Balkan, M C Arikan, S Gokden, V Tilak, B Schaff and R J Shealy, *J. Phys. Condens. Mater.* **14**, 3457 (2002)
[80] N Balkan, R Gupta, M E Daniels, B K Ridley and M Emeny, *Semicond. Sci. Tech.* **5**, 986 (1990)
[81] N Karl, *Organic electronic materials* (Springer, Berlin, Heidelberg, 2001)